Hindawi
International Journal of Antennas and Propagation
Volume 2022, Article ID 2578409, 11 pages
https://doi.org/10.1155/2022/2578409

Research Article

Wideband Patch Antenna with Shorting Vias

Xue Chen [1,2] **and Haipeng Dou** [3]

[1]*Department of Physics, Taiyuan Normal University, Jinzhong, Shanxi, China*
[2]*Institute of Computational and Applied Physics, Taiyuan Normal University, Jinzhong, Shanxi, China*
[3]*Shanxi Vocational University of Engineering Science and Technology, Jinzhong, Shanxi, China*

Correspondence should be addressed to Xue Chen; xuechen0100@sina.com

Received 25 January 2022; Accepted 23 March 2022; Published 1 April 2022

Academic Editor: Ding-Bing Lin

A novel patch antenna with three resonant modes is proposed for wideband applications. By introducing the ring slot on the circular patch, the TM_{02} mode of the smaller circular patch and the TM_{02} mode of the annular ring can be excited. Also, compared with the traditional circular patch with shorting vias, four components of shorting vias are distributed nonuniformly on the edge of the proposed patch antenna, which can generate another new resonance mode. By merging the three resonant modes, the impedance bandwidth of the antenna is expanded. Meanwhile, the gain of the antenna is enhanced in the wide operating band. The results illustrate that the antenna can operate in the 5.8 GHz ISM band. Its −10 dB impedance bandwidth is from 5.06 to 6.99 GHz, and the relative bandwidth reaches 32%. In addition, the maximum gain of 5.3 dBi is obtained at 6.7 GHz.

1. Introduction

With the rapid development of the radio frequency communication technology, the microstrip patch antenna has been widely applied in satellite, radar, remote sensing, and other technical fields because of its simple structure and low cost. However, the conventional patch antennas often have very narrow impedance bandwidths less than 4% because of their single resonance radiation [1, 2]. In this case, many methods have been presented to excite multiple modes for bandwidth improvement of the patch antennas, such as loading parasitic patch [3, 4], etching slot on the patch [5, 6], and introducing shorting vias [7]. In Reference [3], multiple parasitic patches were introduced on the conventional triangular patch antenna, and two more resonances can be obtained. In Reference [4], by introducing four parasitic strips sequentially rotated around the original corner-truncated patch, the −10 dB impedance bandwidth of the antenna reached 630 MHz (24% relative bandwidth). In References [5, 6], ring slots were etched on the circular and square patch antennas, respectively. Two resonances were excited and the broader impedance bandwidths were achieved. In Reference [7], a circular patch antenna with a set of concentric shorting vias was presented, which had two resonances for the TM_{01} and TM_{02} modes.

In addition, several methods were often used in the design of the wideband patch antenna simultaneously [8–10]. For instance, in References [8, 9], both the ring slots and shorting vias were introduced into the design of the circular patch antenna. More than three higher-order modes could be excited. Here, the shorting vias mentioned in these references [7–9] were distributed uniformly around the circular patch to excite the TM_{01} mode. In Reference [10], a ring slot and a series of shorting vias were introduced to merge the TM_{10} and TM_{11} modes excited by the triangular patch antenna.

In this paper, a center-fed wideband patch antenna operating in 5.8 GHz ISM band is proposed. By etching the ring slot on the circular radiation patch, it is decomposed into a smaller circular patch and a coupled annular ring. The TM_{02} mode of the smaller circular patch and the TM_{02} mode of the annular ring can be excited. Then, these two modes are analyzed using the cavity model. Furthermore, some nonuniformly distributed shorting vias are introduced on the edge of the patch. Different from Reference [7–10], these shorting vias are employed to generate another new

resonance mode rather than the TM_{01} mode, which effectively broadens the impedance bandwidth of the antenna. Meanwhile, the gain is enhanced. The measured results indicate that a wide −10 dB impedance bandwidth from 5.06 to 6.99 GHz is realized. Moreover, the gain of the antenna is larger than 3 dBi in this band, and the peak gain reaches 5.3 dBi.

2. Antenna Configuration

Figure 1 shows the configuration of the proposed wideband patch antenna. It consists of a circular radiation patch, a ground plane, and a circular FR4-epoxy substrate ($h = 3.2$ mm, $\varepsilon_r = 4.4$, $\tan\delta = 0.02$). The circular radiation patch with a radius of r_2 is printed on the top of the substrate, and the ground plane is on the other side. A narrow ring slot is etched on the patch, and the patch is decomposed into a smaller circular patch with a radius of a and a coupled annular ring with an inner radius of r_1. Also, twelve shorting vias are loaded on the edge of the circular patch, and each three of them are distributed circumferentially along the $\pm x$ and $\pm y$ directions, respectively. The antenna is centrally fed by a coaxial probe. The optimized structural parameters of the proposed antenna are listed in Table 1.

3. Improvement of the Antenna Bandwidth

In this section, the effect of the annular ring, the ring slot, and the shorting vias on the impedance bandwidth of the antenna is illustrated. Because h (the thickness of the substrate) is very small compared to the wavelength λ_0 in free space, the cavity model can be used to analyze the resonant frequencies of the patch antenna. For the antenna only with smaller circular patch (without slot, annular ring, and shorting vias), the TM_{02} mode can be excited by the central feed. Considering the fringing effect at the open edge, the effective radius a_e of the smaller circular patch can be obtained as follows [7, 11]:

$$a_e = a\sqrt{1 + \frac{2h}{\pi a \varepsilon_r}\left(ln\frac{\pi a}{2h} + 1.7726\right)}. \quad (1)$$

The resonant frequency for the TM_{02} mode is [7]

$$f_{c\mathrm{TM}_{02}} = \frac{3.83171c}{2\pi a_e \sqrt{\varepsilon_r}}, \quad (2)$$

where c is the velocity of light. According to (1) and (2), a_e is 16.16 mm and $f_{c\mathrm{TM}_{02}}$ is 5.4 GHz.

After the annular ring is introduced (with slot and without shorting vias), the TM_{02} mode of the annular ring is excited as well. The resonant frequency for this TM_{02} mode can be calculated by [11]

$$f_{r\mathrm{TM}_{02}} = \frac{c\chi}{2\pi r_1 \sqrt{\varepsilon_r}}, \quad (3)$$

where χ is the root of the characteristic equation [11]. Considering the edge effect, the modified values of the inner and outer radii of the annular ring are given as follows [11]:

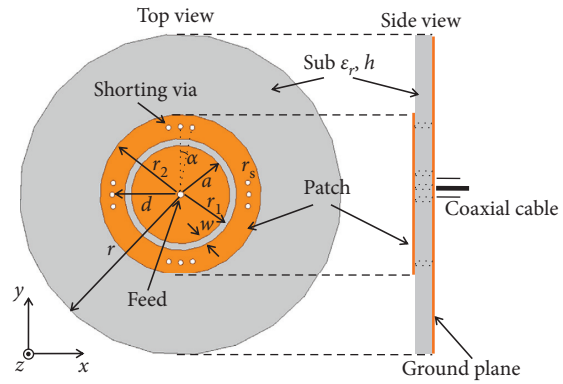

Figure 1: Configuration of the proposed wideband patch antenna.

Table 1: Structural parameters of the antenna (unit: mm).

r	r_1	r_2	a	r_s	w	d	α	h
50	17.4	25	15.3	0.8	2.1	21.2	10°	3.2

$$r_{1e} = r_1 - \frac{3}{4}h,$$
$$r_{2e} = r_2 + \frac{3}{4}h. \quad (4)$$

Then, χ and $f_{r\mathrm{TM}_{02}}$ are calculated by replacing r_1 and r_2 with r_{1e} and r_{2e}, respectively. The calculated χ and $f_{r\mathrm{TM}_{02}}$ are about 3.85 and 5.85 GHz, respectively.

To verify the calculated results of the resonant modes above, Figure 2 shows the simulated input impedance and $|S_{11}|$ of the antenna. In Figure 2(a), for the antenna only with smaller circular patch, it can be seen that the input impedance is about $23 + j0$ Ohm at 5.78 GHz. As a result, the TM_{02} mode of the smaller circular patch is excited here, but the impedance matching is poor as shown in Figure 2(b) because of the strong electric field and the weak magnetic field at the center of the patch. After the annular ring is introduced, the input impedance of the antenna is stable around $50 + j0$ Ohm in the range of 5–6 GHz and two resonances are excited at 5.4 and 6 GHz, corresponding to the TM_{02} mode of the smaller circular patch and the TM_{02} mode of the annular ring, respectively. This shows that the simulated results are in agreement with the calculated ones. Meanwhile, the −10 dB impedance bandwidth reaches 1.45 GHz (5.05–6.5 GHz) because these two adjacent resonant frequencies are close to each other.

When the shorting vias are also introduced, the third mode is excited at 6.8 GHz. The resonant frequency of this mode is higher than that of the TM_{02} mode of the annular ring and lower than that of its TM_{12} mode, which is different from the TM mode of the cylindrical cavity. By adjusting the position and number of the shorting vias, the resonant frequency of the third mode can be controlled and the three bands corresponding to these three modes can merge into a broadband. As shown in Figure 2(a), the input resistance around 6.8 GHz is increased to 50 Ohm after the shorting

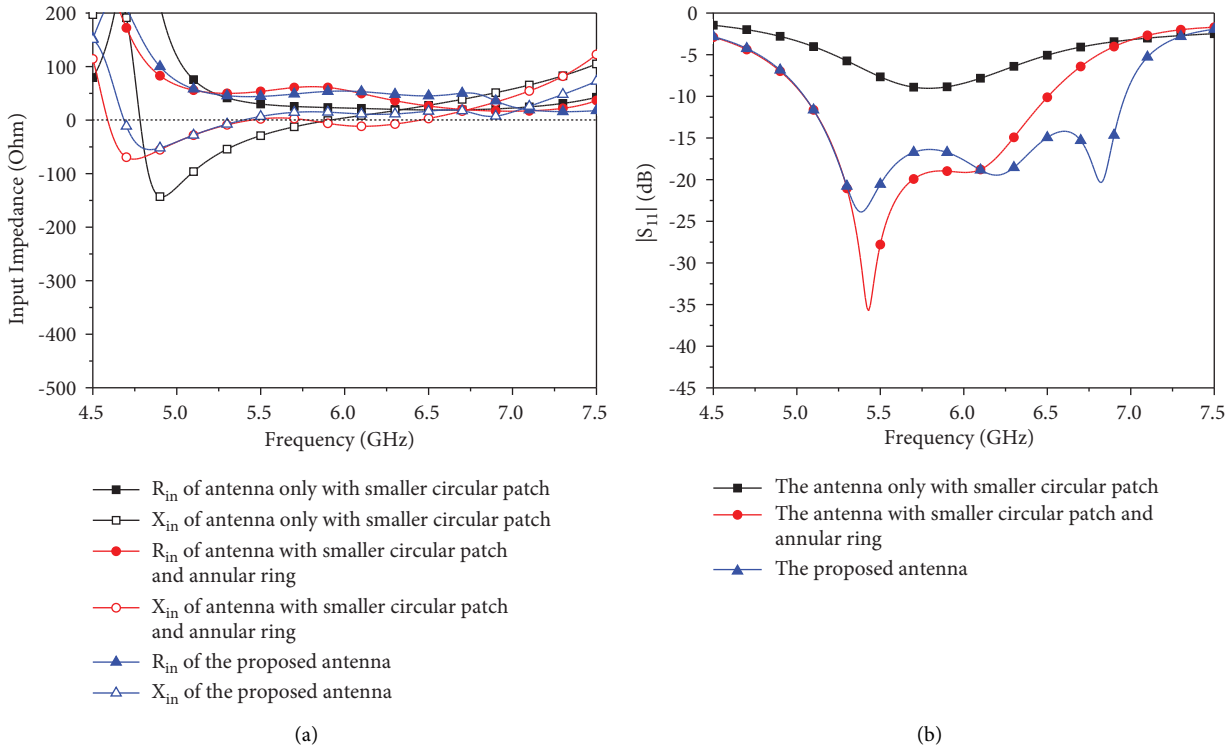

FIGURE 2: Simulated input impedance and $|S_{11}|$ without and with annular ring and shorting vias. (a) Input impedance. (b) $|S_{11}|$.

vias are introduced. This is because an additional equivalent resistance is loaded on the edge of the patch. Meanwhile, adjacent vias give rise to a parallel inductance, which results in a decrease of the input reactance at this frequency band. In this case, the input impedance of the antenna in the range of 6–7 GHz is also stable around $50 + j0$ Ohm and a broadband from 5.05 to 6.97 GHz is achieved, as shown in Figure 2(b).

In addition, the current distribution on the patch for these three modes is exhibited in Figure 3. At 5.4 GHz, for the TM_{02} mode of the smaller circular patch, the current flows from the center of the patch to the inner side of the ring slot. At 6.2 GHz, for the TM_{02} mode of the annular ring, the current flows from the outer edge to inner edge of the annular ring. At 6.8 GHz, for the third mode, the current on the patch between two sets of adjacent shorting vias is almost homodromous (as the blue arrow shown). This means that the magnetic field in this region is continuous. On the contrary, the current around the shorting vias is reversed (as the black arrow shown), which indicates that the magnetic field in this region is discontinuous and some current passes through the shorting vias.

Next, the influence of r_1, w, and d, and the number of shorting via on the performance of antenna is studied. The results are shown in Figures 4–7. Figure 4 shows the $|S_{11}|$ of the proposed antenna for different r_1. When r_1 is 16.4 mm, the TM_{02} mode of annular ring is not excited and two separate bands corresponding to the center frequencies of 5.25 and 6.5 GHz are formed, respectively. Then, with the increase of r_1, the resonant frequency for the third mode shifts up. When r_1 is 17.4 mm, three adjacent bands at 5.4, 6.2, and 6.8 GHz merge into a whole one from 5.05 to 6.97 GHz. However, as r_1 increases to 18.4 mm, the $|S_{11}|$ exceeds −10 dB at 6.5 GHz, and the TM_{02} mode of annular ring is lost again.

Figure 5 shows the $|S_{11}|$ for different w. It can be seen that a narrow operating band of 5.34–6.87 GHz ($|S_{11}| < -10$ dB) is obtained when w is 3.1 mm. Then, the resonant frequency for the TM_{02} mode of the smaller circular patch (the first resonance) shifts down with the decrease of w and the bandwidth is broadened. Nevertheless, when w decreases to 1.1 mm, the operating band is divided into two separate bands.

Figure 6 shows the $|S_{11}|$ for different d. It can be seen that when d is 22.2 mm, there is no third mode. With the decrease of d, this mode is excited and the bandwidth of the antenna is broadened. However, when d decreases to 20.2 mm, two separate bands are observed.

Finally, Figure 7 shows the $|S_{11}|$ for different numbers of shorting vias. It can be seen that the number of shorting vias has effect on both the TM_{02} mode of the smaller circular patch and the third mode. No matter one or five shorting vias are introduced along the $\pm x$ and $\pm y$ directions, only two resonances can be excited. For example, when a shorting via is introduced, the third mode cannot be excited and the antenna has an operating band of 5.01–6.52 GHz. When the number of the shorting vias increases to five, the resonance at 5.3 GHz for the TM_{02} mode of the smaller circular patch disappears and the third mode is excited at 6.8 GHz. The center frequency of the antenna shifts up to 6.23 GHz and the bandwidth is from 5.43 to 7.02 GHz. Only when three shorting vias are introduced, three resonances at 5.4, 6.2, and 6.8 GHz can be observed and the widest bandwidth is

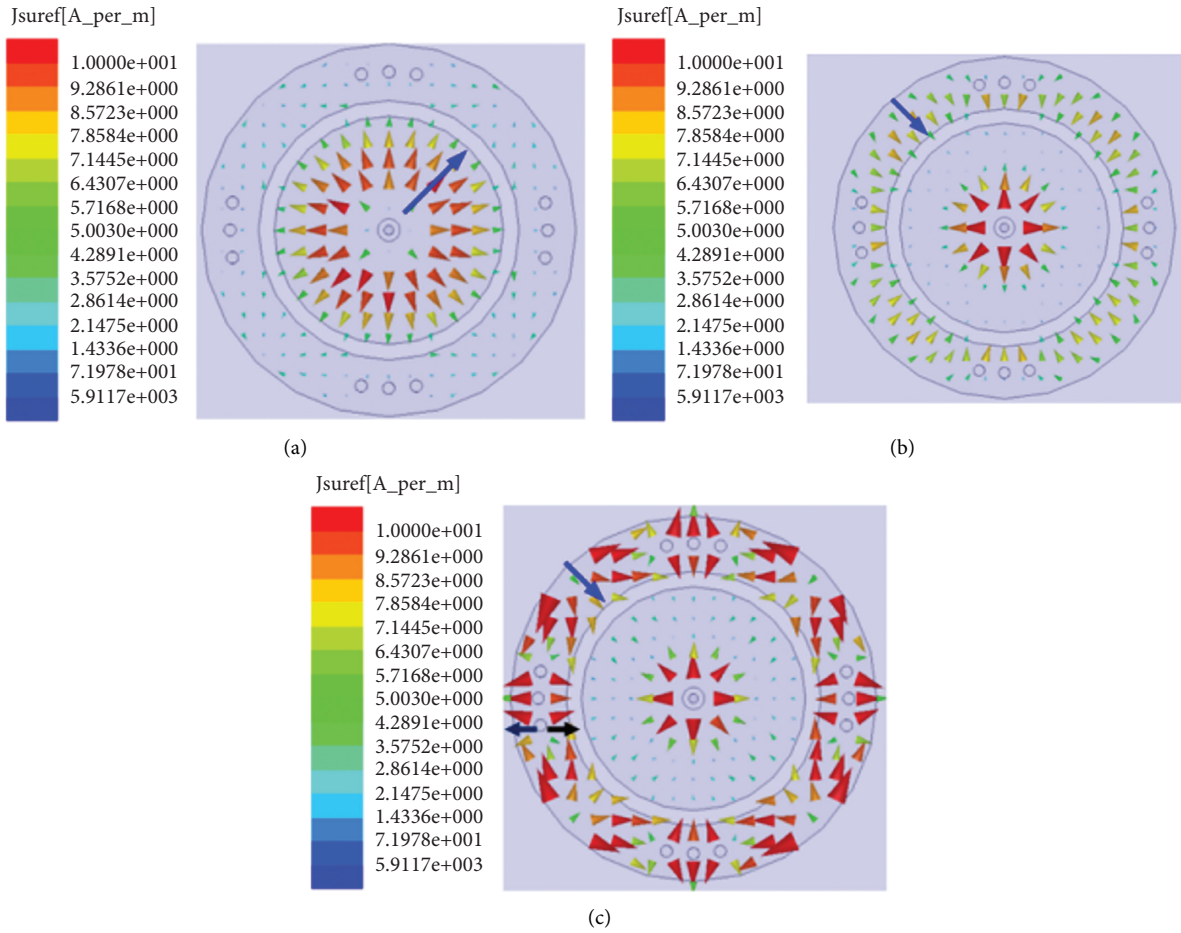

Figure 3: The current distribution on the patch. (a) 5.4 GHz, (b) 6.2 GHz, and (c) 6.8 GHz.

obtained. Overall, $r_1 = 17.4$ mm, $w = 2.1$ mm, and $d = 21.2$ mm, and three shorting vias are chosen and the −10 dB impedance bandwidth of the antenna is from 5.05 to 6.97 GHz.

4. Improvement of the Antenna Gain

The annular ring and the shorting vias also affect the gain of the proposed antenna, as shown in Figure 8. For brevity, Figure 9 gives the electric field distribution in these three cases at 6.7 GHz in *xoz* plane. For the antenna only with the smaller circular patch, it is noticed that the gain is high at around 6 GHz and the maximum gain reaches 3.25 dBi. Nevertheless, with the decrease of the frequency, the gain decreases sharply. Also, the energy of the radiation field is mainly concentrated on the smaller circular patch as shown in Figure 9(a).

After the annular ring is introduced, the gain in the range of 5–5.6 GHz is enhanced to 2.5 dBi. Meanwhile, in the range of 6–6.8 GHz, the gain is also enhanced. This is because that the energy in the inner side of the ring slot is coupled into the annular ring and the effective radiation aperture of the antenna is enlarged, as shown in Figure 9(b). When the shorting vias are also introduced, the gain is enhanced obviously in the band of 5.5–7 GHz and a peak gain of 5.4 dBi appears at 6.7 GHz. This is because the input impedance of the antenna gets matched in this band after the shorting vias are introduced (as shown in Figure 2(a)), which results in a decrease in the reflected energy of the antenna and an increase in the radiated energy, as shown in Figure 9(c). Thus, the gain is improved.

5. Simulated and Measured Results

To validate the simulated results, a prototype of the antenna with the optimized parameters is fabricated and measured. Figure 10 shows its photographs, and the measured results are shown in Figures 11–14. Figure 11 shows the $|S_{11}|$ of the proposed antenna. The measured impedance bandwidth ($|S_{11}| < -10$ dB) is 32% (5.06–6.99 GHz), which is in agreement with the simulated one.

Figures 12–14 show the normalized radiation patterns at 5.4, 6.2, and 6.8 GHz, respectively. A good agreement between the simulated and measured results is achieved. It can be seen that the conical-beam radiation patterns are observed in the elevation ($\varphi = 0^\circ$) plane. The maximum radiation is at the angles of $\theta = 50^\circ$ and 310°. At these three frequencies, the half-power beamwidths of the antenna are 70°, 40°, and 50°, respectively. This indicates that the radiation gains variation against these angles of θ are almost identical. In the azimuth plane of $\theta = 50^\circ$, the omnidirectional radiation characteristics are achieved at 5.4

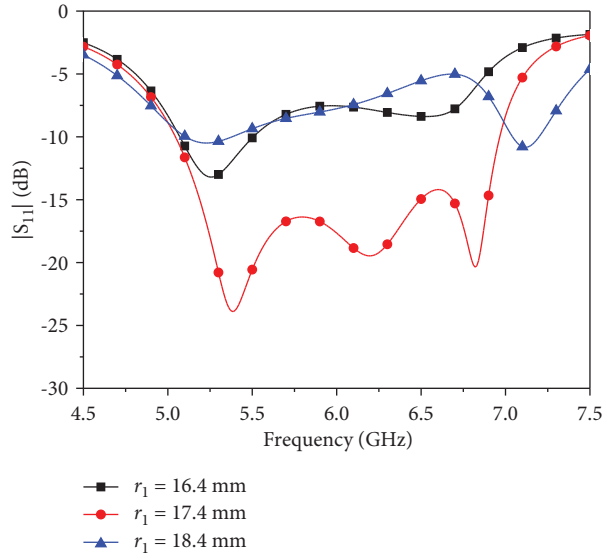

Figure 4: $|S_{11}|$ of the proposed antenna for different r_1.

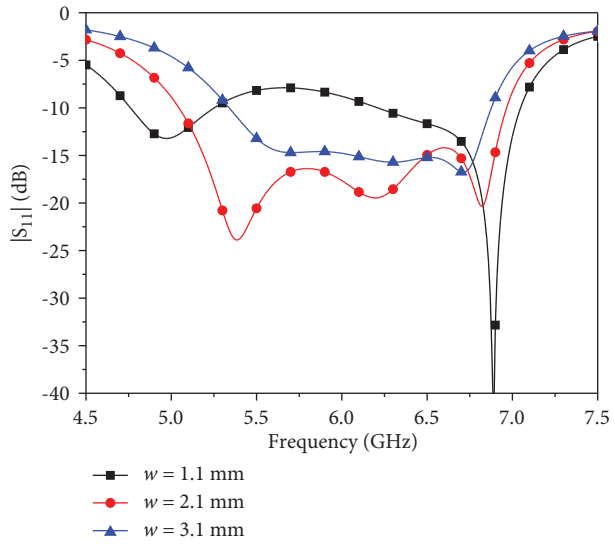

Figure 5: $|S_{11}|$ of the proposed antenna for different w.

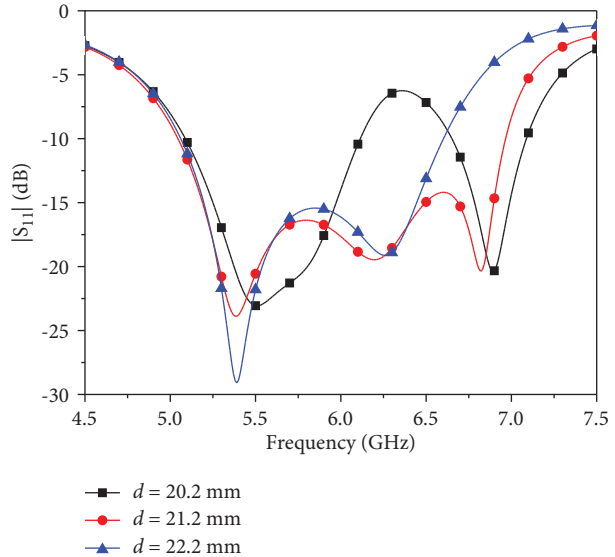

Figure 6: $|S_{11}|$ of the proposed antenna for different d.

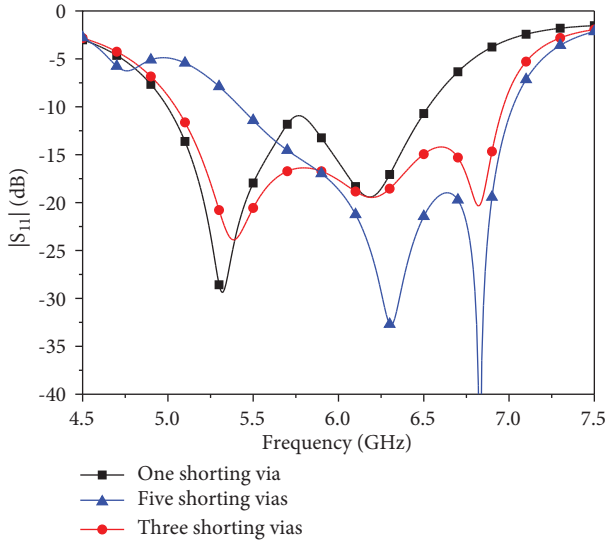

Figure 7: $|S_{11}|$ of the antenna for different numbers of vias.

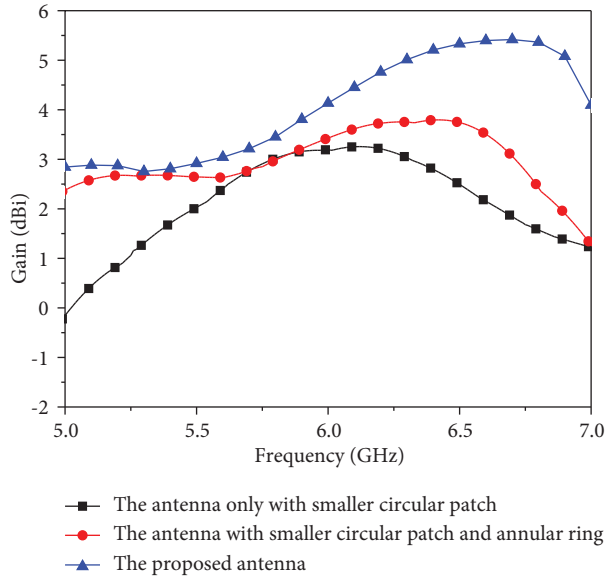

Figure 8: Simulated gain of the antenna without and with annular ring and shorting vias.

and 6.2 GHz. However, at 6.8 GHz, the antenna has the larger radiation at the angles of $\varphi = 0^\circ$, 90°, 180°, and 270° due to the introduction of the shorting vias along the $\pm x$ and $\pm y$ directions. Moreover, the cross-polarization radiation in the azimuth plane is larger than that in elevation plane. Nevertheless, it is still less than −15 dB. In addition, the similar radiation patterns have also been obtained in the other azimuth planes of $\theta = 20^\circ$–70°. Therefore, they are not included here.

Figure 15 shows the gain of the antenna. The measured gain is stable and larger than 4 dBi in the range of 6–7 GHz. The peak gain of 5.3 dBi is obtained at 6.7 GHz. It also can be seen that the gain in the band of 5–6 GHz is lower. This is because the proposed antenna has a wider half-power beamwidth ($\theta = 20^\circ$–70°) in this band. Also, in the azimuth planes of $\theta = 20^\circ$–70°, the radiation for all the φ is nearly equal, which results in a wider radiation range and a lower gain in this band. Moreover, the measured efficiency of the antenna is also shown in Figure 15, which varies between 65% and 88% in the band of 5.06–6.99 GHz.

Finally, the related wideband patch antennas are listed in Table 2. These antennas that use the slot and shorting vias to improve the bandwidth all have larger sizes.

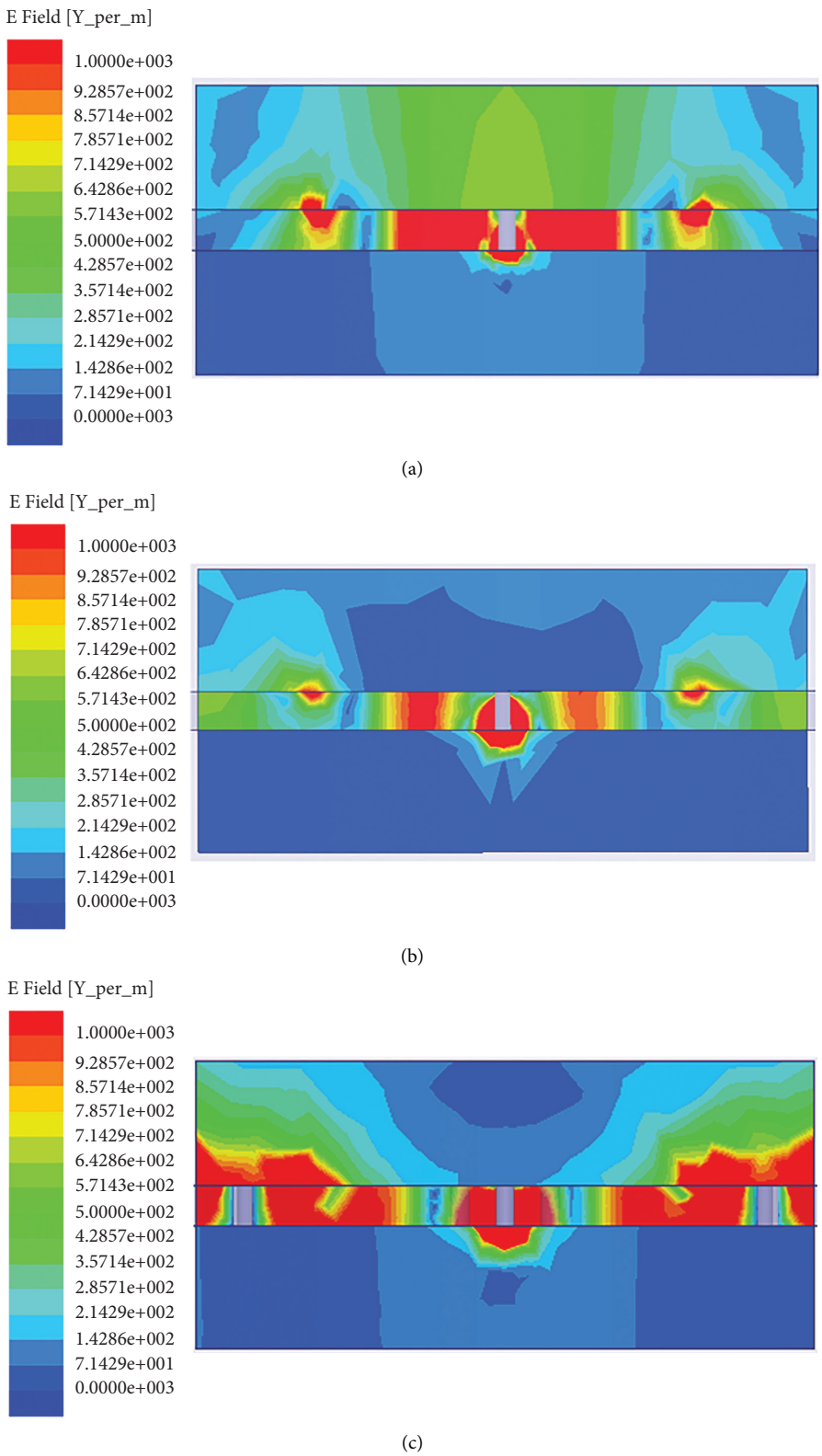

FIGURE 9: The electric field distribution of the antenna at 6.7 GHz in *xoz* plane. (a) Only with smaller circular patch, (b) with smaller circular patch and annular ring, and (c) the proposed antenna.

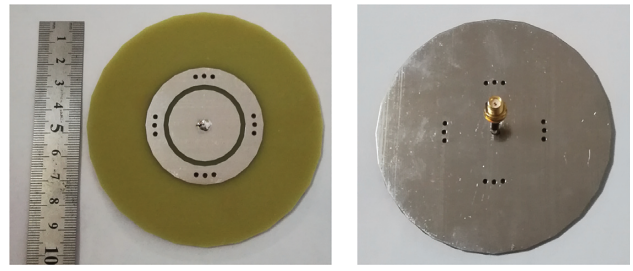

(a) (b)

Figure 10: Photos of the proposed antenna. (a) The top view. (b) The bottom view.

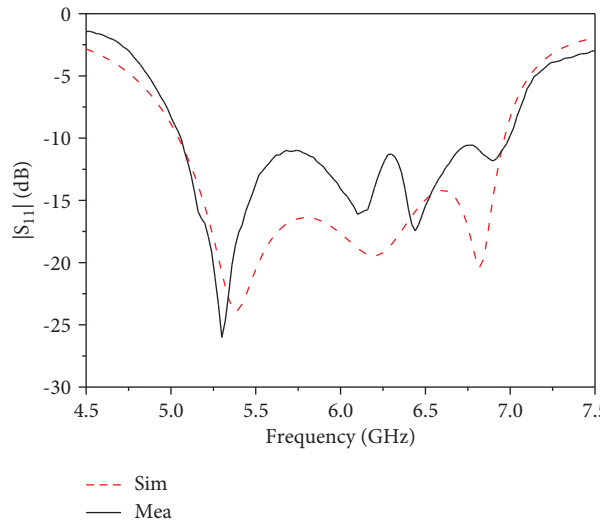

Figure 11: Simulated and measured $|S_{11}|$ of the proposed antenna.

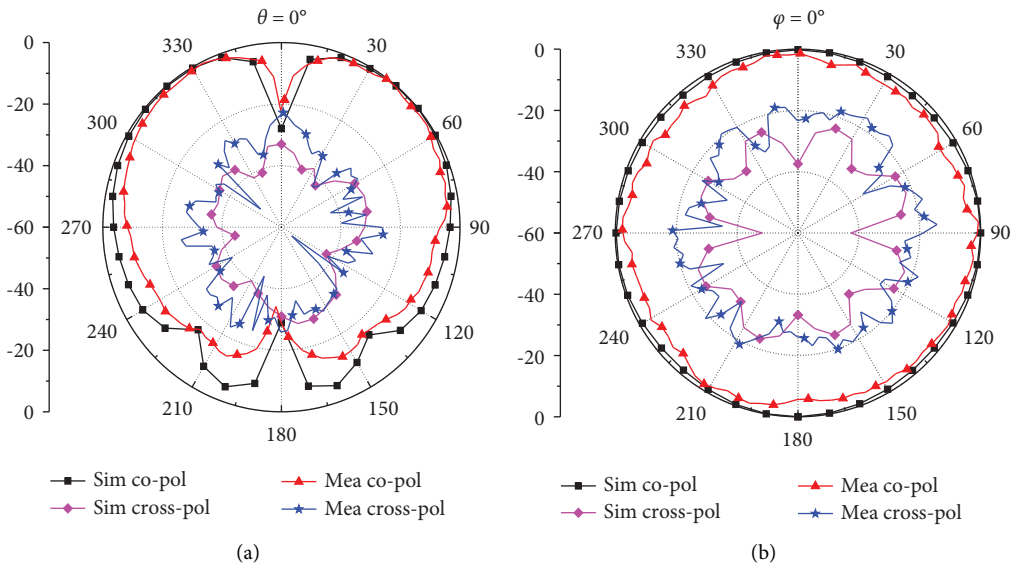

Figure 12: Simulated and measured radiation patterns at 5.4 GHz. (a) $\varphi = 0^{\circ}$ (x-z plane). (b) $\theta = 50^{\circ}$.

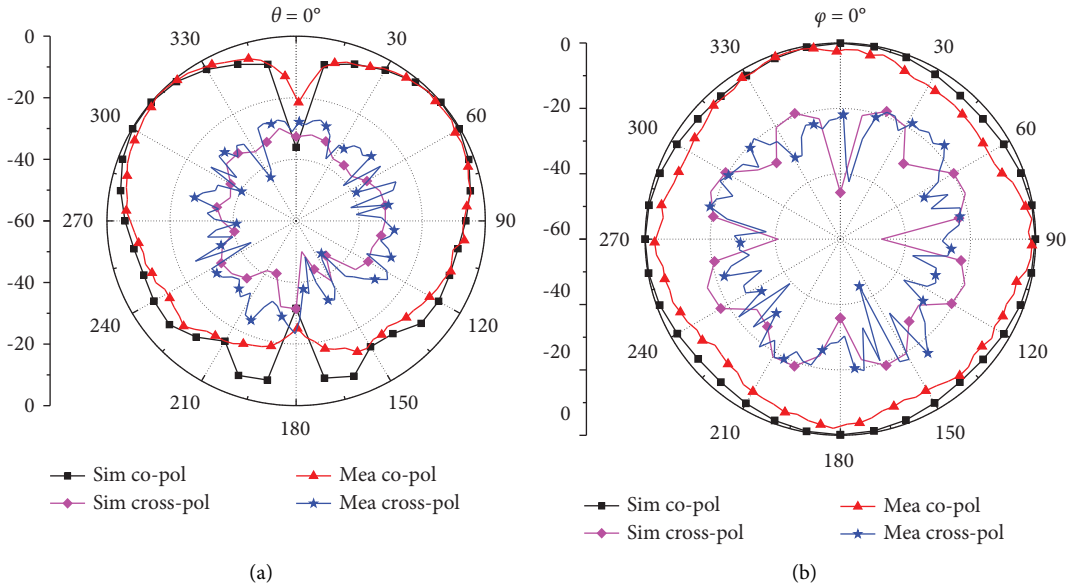

Figure 13: Simulated and measured radiation patterns at 6.2 GHz. (a) $\varphi = 0^{\circ}$ (x-z plane). (b) $\theta = 50^{\circ}$.

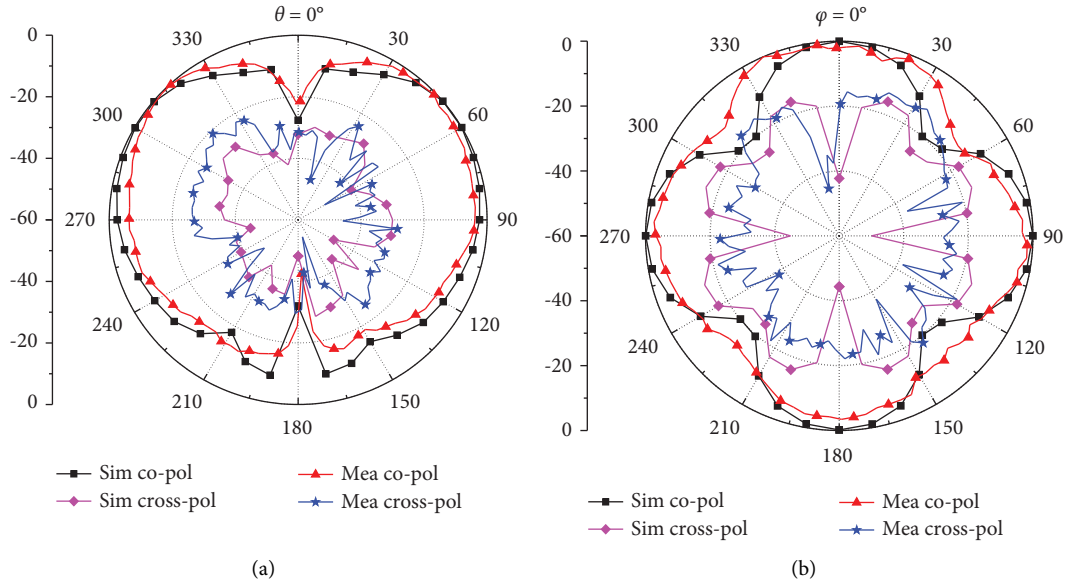

Figure 14: Simulated and measured radiation patterns at 6.8 GHz. (a) $\varphi = 0^{\circ}$ (x-z plane). (b) $\theta = 50^{\circ}$.

However, compared with these designs in References [5–10], a new method of loading nonuniformly distributed shorting vias is used to excite another resonance to broaden the bandwidth, and the proposed patch antenna has the widest impedance bandwidth (except the one in Reference [6], which has a higher profile).

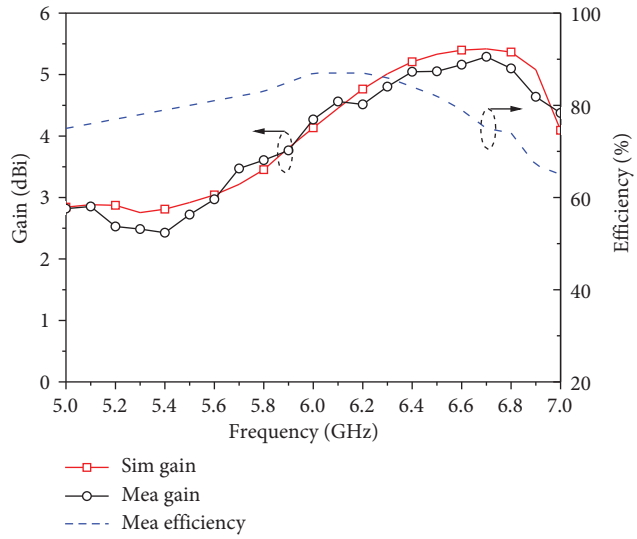

Figure 15: Gain and efficiency of the antenna.

Table 2: Comparison of the wideband patch antennas.

	Electrical dimension	Center frequency (GHz)	Relative bandwidth (%)	Shape of patch	Method of improving bandwidth
Reference [5]	$2.9\lambda_0 \times 2.9\lambda_0 \times 0.029\lambda_0$	5.8	12.8	Circle	Slot
Reference [6]	$1.12\lambda_0 \times 1.12\lambda_0 \times 0.09\lambda_0$	3.37	70	Square	Slot and shorting wall
Reference [7]	$1.35\lambda_0 \times 1.35\lambda_0 \times 0.024\lambda_0$	2.26	18	Circle	Shorting vias
Reference [8]	$2.34\lambda_0 \times 2.34\lambda_0 \times 0.029\lambda_0$	5.85	27.4	Circle	Slot and shorting vias
Reference [9]	$1.05\lambda_0 \times 1.05\lambda_0 \times 0.048\lambda_0$	2.42	11.2	Circle	Slot and shorting vias
Reference [10]	$1.48\lambda_0 \times 1.48\lambda_0 \times 0.03\lambda_0$	4.5	8.9	Triangle	Slot and shorting vias
This work	$2\lambda_0 \times 2\lambda_0 \times 0.064\lambda_0$	6.03	32	Circle	Slot and shorting vias

λ_0, wavelength at the center frequency.

6. Conclusion

In this paper, a wideband patch antenna with ring slot and nonuniformly distributed shorting vias is proposed. The ring slot is utilized to simultaneously excite the TM_{02} mode of the smaller circular patch and the TM_{02} mode of the annular ring. Meanwhile, the nonuniformly distributed shorting vias is introduced to generate the third resonance mode. A wider bandwidth can be achieved by coupling three modes. The results show that this antenna has a broad bandwidth of 5.06–6.99 GHz and its maximum gain reaches 5.3 dBi. It is compact and can be applied to the 5.8 GHz ISM band.

Data Availability

Data sharing not applicable to this article as no datasets were generated or analyzed during the current study.

Conflicts of Interest

The authors declare that they have no conflicts of interest.

Acknowledgments

This work was supported by the Scientific and Technological Innovation Programs of Higher Education Institutions in Shanxi (2020L0501).

References

[1] L. Economou and R. J. Langley, "Patch antenna equivalent to simple monopole," *Electronics Letters*, vol. 33, no. 9, pp. 727–729, 1997.

[2] Z. Yang, K. C. Browning, and K. F. Warnick, "High-efficiency stacked shorted annular patch antenna feed for Ku-band satellite communications," *IEEE Transactions on Antennas and Propagation*, vol. 64, no. 6, pp. 2568–2572, 2016.

[3] K. D. Xu, H. Xu, Y. Liu, J. Li, and Q. H. Liu, "Microstrip patch antennas with multiple parasitic patches and shorting vias for bandwidth enhancement," *IEEE Access*, vol. 6, pp. 11624–11633, 2018.

[4] J. Wu, Y. Yin, Z. Wang, and R. Lian, "Broadband circularly polarized patch antenna with parasitic strips," *IEEE Antennas and Wireless Propagation Letters*, vol. 14, pp. 559–562, 2015.

[5] A. Al-Zoubi, F. Yang, and A. Kishk, "A broadband center-fed circular patch-ring antenna with a monopole like radiation pattern," *IEEE Transactions on Antennas and Propagation*, vol. 57, no. 3, pp. 789–792, 2009.

[6] S.-J. Lin and J.-S. Row, "Monopolar patch antenna with dual-band and wideband operations," *IEEE Transactions on Antennas and Propagation*, vol. 56, no. 3, pp. 900–903, 2008.

[7] J. Liu, Q. Xue, H. Wong, H. W. Lai, and Y. Long, "Design and analysis of a low-profile and broadband microstrip monopolar patch antenna," *IEEE Transactions on Antennas and Propagation*, vol. 61, no. 1, pp. 11–18, 2013.

[8] J. Liu, S. Zheng, Y. Li, and Y. Long, "Broadband monopolar microstrip patch antenna with shorting vias and coupled ring," *IEEE Antennas and Wireless Propagation Letters*, vol. 13, pp. 39–42, 2014.

[9] Z. Liang, J. Liu, Y. Li, and Y. Long, "A dual-frequency broadband design of coupled-fed stacked microstrip monopolar patch antenna for WLAN applications," *IEEE Antennas and Wireless Propagation Letters*, vol. 15, pp. 1289–1292, 2016.

[10] T. L. Wu, Y. M. Pan, P. F. Hu, and S. Y. Zheng, "Design of a low profile and compact omnidirectional filtering patch antenna," *IEEE Access*, vol. 5, pp. 1083–1089, 2017.

[11] R. Garg, P. Bhartia, I. Bahl, and A. Ittipiboon, *Microstrip Antenna Design Handbook*, pp. 324–372, Artech House, Norwood, MA, USA, 2001.